Article:
Wei, W, Ettelaie, R orcid.org/0000-0002-6970-4650, Zhang, X et al. (4 more authors) (2022) Co-compartmentalization of Enzymes and Cofactors within Pickering Emulsion Droplets for Continuous Flow Catalysis. Angewandte Chemie International Edition, 61 (45). e202211912. ISSN 1433-7851

https://doi.org/10.1002/anie.202211912

Co-compartmentalization of Enzymes and Cofactors within Pickering Emulsion Droplets for Continuous Flow Catalysis

Wei Wei, Rammile Ettelaie, Xiaoming Zhang, Min Fan, Yue Dong, Zebiao Li, and Hengquan Yang*

Abstract: *Co-immobilization of enzymes and cofactors in a manner suitable for use in continuous flow catalysis remains a great challenge because of the difficulty in ensuring the free accessibility of immobilized enzymes and cofactors. Herein, we present a continuous flow catalysis system based on co-compartmentalization of enzymes and cofactors within Pickering emulsion droplets, which can realize co-immobilized enzymes and cofactors and regeneration of cofactors within the droplets. As exemplified by enzyme-catalyzed ketone enantioselective reduction and enantioselective transamination, our systems exhibit long-term stability (300-400 h), outstanding total turnover number (TTN, 59204 mol mol^{-1}) and several-fold enhancement in the enzyme catalytic efficiency (CE_e) in comparison to conventional biphasic reactions. Our method along with revealing insight into the co-compartmentalization effects will provide a vast opportunity for significantly advancing continuous flow biocatalysis towards the level of practical applications.*

Introduction

Continuous flow biocatalysis is emerging as a very promising means to upgrade current chemical synthesis because it integrates two enabling technologies: biocatalysis and continuous flow reaction.[1] Such an integration makes it possible to reconcile many noteworthy advantages such as high enantioselectivity,[1a-e] enhanced reaction efficiency[1f-i] and simplified downstream treatment.[1e,h] Despite being very appealing for practical applications, the continuous flow biocatalysis remains at the cutting edge of science and technology development since there remain many critical challenges, for example efficient immobilization of enzymes and long-term operational stability.[2] More challenging is the immobilization of cofactor-dependent enzymes because the co-immobilization of enzymes and cofactors often sacrifices their mutual accessibility.[3] Since cofactor-dependent enzymatic reactions are very popular in biocatalysis and moreover most cofactors such as nicotinamide adenine dinucleotide phosphate (NADPH) and pyridoxal 5-phosphate monohydrate (PLP) are very expensive, development of a more elegant and practical method to co-immobilize enzymes and cofactors for efficient continuous flow biocatalysis is of paramount importance.[3a,b]

In pursuit of this goal, extensive efforts have been made in past years.[4] For instance, transaminases were grafted onto polyethyleneimine-modified agarose microbeads, in which the cofactors are retained through ion-pair interactions.[4a] The dynamic equilibriums of dissociation-association make the enzymes and cofactors come transiently into contact with each other. Mycobacterium smegmatis acetate kinases and the relevant cofactors were fused on DNA frameworks, in which a flexible swinging arm allows the enzyme and cofactor to access each other.[4b] Enzymes and cofactors were co-grafted on inorganic supports or insoluble polymers functionalized with reactive groups, where the flexible spacers are expected to render them accessible.[4c,d] Although the obtained results are very encouraging, there remains a big gap between these existing co-immobilization techniques and an ideal immobilization method, which should ensure unrestricted accessibility between enzymes and cofactors, be self-sufficient (without need for exogenous cofactors), and provide a physiological microenvironment for enzymes.[4e-j]

Pickering emulsions (using nanoparticles as emulsifiers instead of surfactants) are emerging as an important platform for biphasic catalysis.[5] In our recent work, micron-sized Pickering emulsion droplets were shown to be capable of being packed in column reactors for continuous flow reactions owing to their high droplet stability to coalescence.[6] Here, we advance one further step forwards by exploring the unique interfacial adsorption and confinement effects offered by Pickering emulsion droplets to co-compartmentalize enzymes and cofactors, leading to an elegant co-immobilization strategy for continuous flow biocatalysis. As Figure 1A shows, an organic/water biphasic system containing enzymes and cofactors is transformed to a water-in-oil (W/O) Pickering emulsion through emulsification, generating numerous water droplets within which the enzymes and cofactors are co-compartmentalized. The resultant Pickering emulsion droplets are then packed in a column reactor, generating a fixed-bed reactor for continuous flow reactions. The interspaces among droplets allow a substrate-containing oil phase to flow down around the droplet interfaces where catalytic reactions take place. During the continuous flow reaction, the enzymes always reside at the droplet interfaces due to their high affinity for adsorption at the droplet interfaces. At the same time, water-soluble cofactors remain confined within the droplets thanks to their high water solubility (low solubility in the oil phase), but can unrestrictedly access enzymes adsorbed at the droplet interfaces since the dissolved cofactor molecules can move freely within the droplets. Moreover, the cofactors within the droplets can be fully regenerated through co-substrate-involved enzymatic reactions (Figure 1A, middle). Consequently, the enzyme and cofactor are "co-immobilized" in the continuous flow reactor and work under a physiological microenvironment, exhibiting exceptional

[*] W. Wei, X. Zhang, M. Fan, Y. Dong, Prof. H. Yang
School of Chemistry and Chemical Engineering
Shanxi University
Taiyuan 030006 (China)
E-mail: hqyang@sxu.edu.cn

Dr. R. Ettelaie
Food Colloids Group, School of Food Science and Nutrition
University of Leeds
Leeds LS2 9JT (UK)

Dr. Z. Li
Nantong Chanyoo Pharmatech Co., Ltd.
Nantong 226400 (China)

Supporting Information for this article is given via a link at the end of the document.

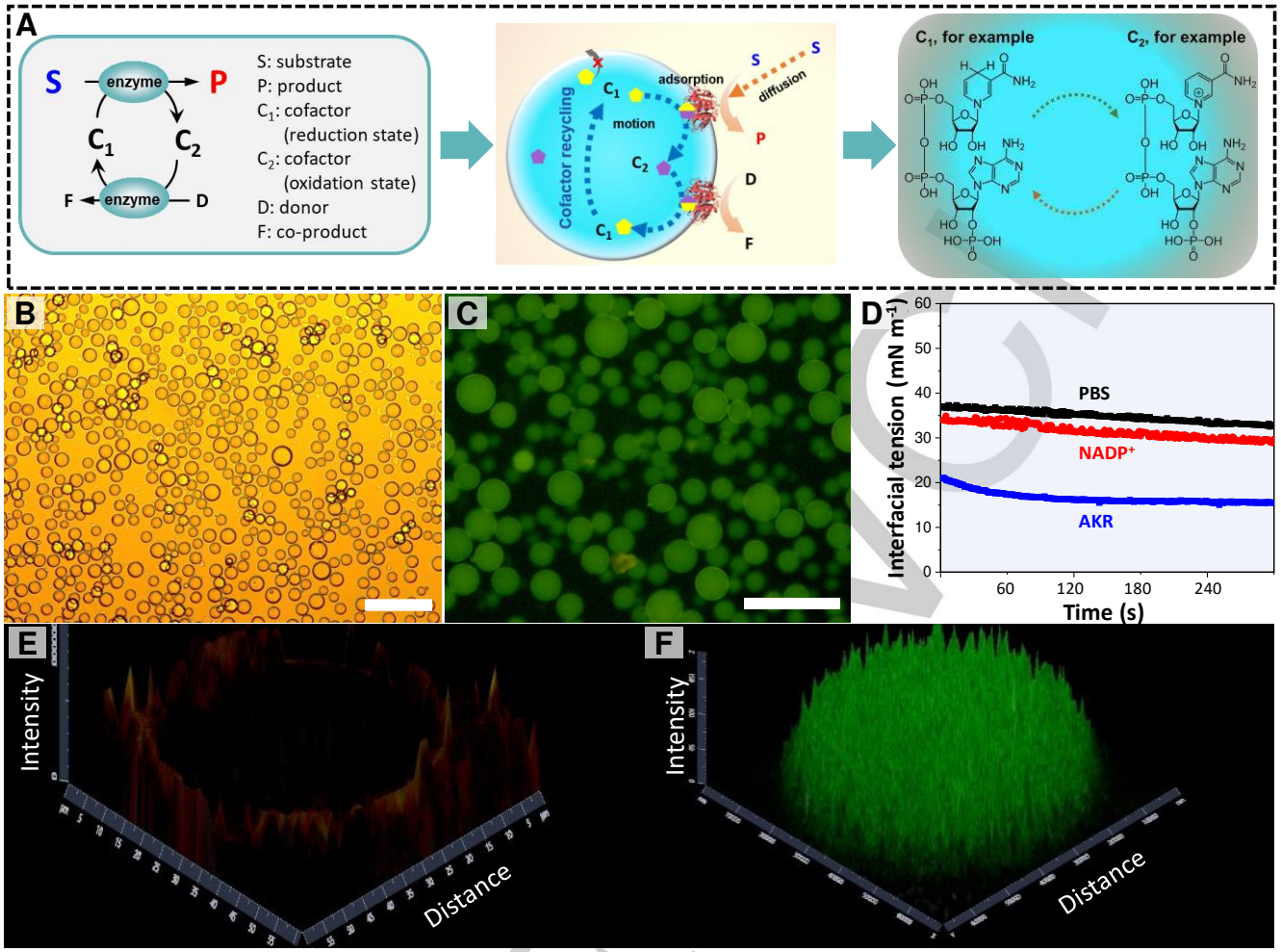

Figure 1. Characterizations for the co-compartmentalization of enzymes and cofactors within Pickering emulsion droplets. A) Schematic illustration of the principle for the co-compartmentalization of enzymes and cofactors within a Pickering emulsion droplet. B) Optical microscopy image for the formed Pickering emulsion droplets. C) Fluorescence confocal microscopy image of the droplets which were dyed with water-soluble FITC-dextran. D) Dynamic interfacial tension of the water/*n*-heptane in the presence of enzyme or cofactor, AKR (0.58 mg mL^{-1} of protein, 0.92 U mg^{-1}) or $NADP^+$ (80 μM), PBS as background. E) 2.5D confocal fluorescence microscopy showing location of Rhodamine B-labelled AKR at the droplet interface. F) 2.5D confocal fluorescence microscopy showing the location of NADPH within the Pickering emulsion droplet. Scale bar = 100 μm.

performances. The essential advance both in terms of co-compartmentalizing enzymes/cofactors and reusing enzymes/cofactors would definitely benefit practical applications of biocatalysis.

Results and Discussion

We chose enantioselective ketone reduction to examine our system since this reaction involves a reductase and its cofactor NADPH (i.e. the corresponding reductive state of $NADP^+$, Figure 1A) and thus represents a typical cofactor-dependent enzymatic reaction.[4a-c,g,7] Notably, an aldo-keto reductase (AKR, Figure S1) used here can catalyze the co-substrate-involved reaction besides the substrate-involved reaction, regenerating the cofactor (Figure 1A). A biphasic mixture of PBS (phosphate buffer: 0.1 M Na_2HPO_4, 0.1 M NaH_2PO_4, pH 7.4) solution, *n*-heptane, AKR and cofactors ($NADP^+$) was emulsified in the presence of partially hydrophobic silica nanoparticles as emulsifiers (with an average particle size of 60 nm; transmission electron microscopy images, N_2 sorption isotherms, contact angle measurement results and thermogravimetric analysis for the emulsifiers are displayed in Figure S2). As the optical micrograph in Figure 1B shows, the resultant Pickering emulsion droplets are uniform in shape with an average diameter of 41 μm. The type of water-in-oil emulsion was confirmed by a fluorescent experiment with water staining (Figure 1C). In order to know where the enzymes and cofactors locate within the Pickering emulsion system, we measured dynamic interfacial tension between water and oil phases in the presence of enzymes or cofactors using pendant drop tensiometry. As displayed in Figure 1D, the approximate equilibrium interfacial tension of PBS buffer/*n*-heptane (as background) was measured to be 35 mN m^{-1}. However, after adding AKR into this system (0.58 mg mL^{-1} of protein, 0.92 U mg^{-1}, see Experimental Section in SI), the equilibrium interfacial tension dramatically decreased down to 15 mN m^{-1}. This decrease in interfacial tension indicates that AKR has a strong propensity to adsorb at the oil/water interfaces.[8] To gain more information on the adsorption of AKR at the interfaces, we further measured the dynamic interfacial tensions of PBS buffer/*n*-heptane in the presence of different concentrations of AKR (Figure S3a). As the AKR concentration increased from 0.036 to 0.725 mg mL^{-1}, the interfacial tension decreased from 33 to 13 mN m^{-1}. However, further increasing the AKR concentration did

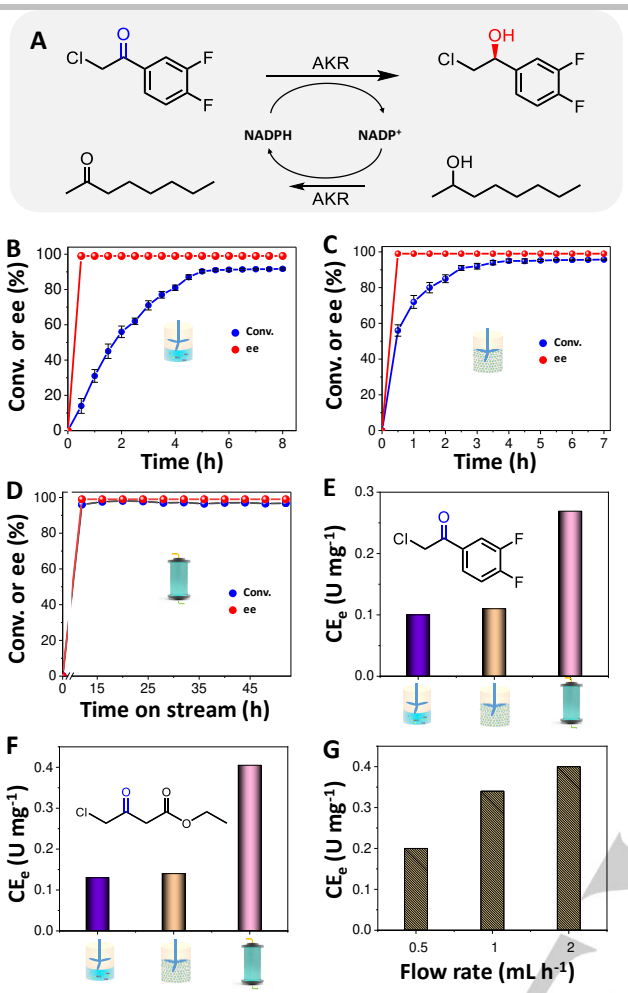

Figure 2. Comparison of the enzymatic ketone reductions in batch and continuous flow systems. A) Enantioselective reduction of 2-chloro-3',4'-difluoroacetophenone. B-D) Kinetic profiles for 2-chloro-3',4'-difluoroacetophenone reduction in different systems: B) Conventional biphasic system in batch. C) Pickering emulsion system in batch. D) Pickering emulsion-based continuous flow system. E) Comparisons of the catalytic efficiencies of AKR in different systems using 2-chloro-3',4'-difluoroacetophenone as substrate. F) AKR catalytic efficiencies towards the reduction of ethyl 4-chloroacetoacetate in different systems. G) Catalytic efficiencies of AKR in Pickering emulsion-based continuous flow systems with different flow rates. Reaction conditions for the conventional biphasic reaction in batch: 3.6 mL of aqueous AKR (0.58 mg mL^{-1}) and NADP$^+$ (80 μM), 1.8 mL of *n*-heptane containing 2-chloro-3',4'-difluoroacetophenone (0.1 M) and 2-octanol (0.24 M), 30 °C, 600 rpm. The reaction conditions for Pickering emulsion system in batch are the same as those for the conventional biphasic reaction except that 0.15 g emulsifier was added to formulate the Pickering emulsion. Reaction conditions for the Pickering emulsion-based continuous flow system: Pickering emulsion consists of 1.8 mL of *n*-heptane, 3.6 mL of aqueous AKR (0.58 mg mL^{-1}) and NADP$^+$ (80 μM) and 0.15 g of emulsifier, 0.10 M 2-chloro-3',4'-difluoroacetophenone and 0.24 M 2-octanol in *n*-heptane, 30 °C, 0.5 mL h^{-1}. The catalytic efficiency of enzyme (CE_e, U mg^{-1}) is defined as μmol of substrate converted per milligram of enzyme per min. For batch reactions, CE_e is estimated when the substrate approaches a nearly full conversion (within the first 7 h in this work); for continuous flow reactions, CE_e is calculated at steady state (μmol of substrate converted within 60 min per milligram of enzyme per 60 min). The catalytic efficiencies of AKR were calculated according to the conversions within the first 7 h for the batch reactions, and after the conversion leveled off for the continuous flow reactions.

not lead to any apparent reduction of the equilibrium interfacial tension. This is a likely indication that the interfacial adsorption reached saturation, completing a "monolayer" adsorption at the interfaces.[8] In contrast to AKR, NADP$^+$ did not tend to migrate towards the oil/water interfaces, with the equilibrium interfacial tension showing no significant decrease after addition of NADP$^+$ into the system (Figure S3b). This means that NADP$^+$ molecules are homogeneously distributed within the bulk water phase rather than at interfaces. This is a reasonable proposition because NADP$^+$ itself is highly water-soluble, bearing multiple polar groups and one charged group (Figure 1A). To further confirm the precise location of the enzymes and cofactors in the Pickering emulsion system, fluorescence confocal microscopy experiments were performed.[4c,9] It was found that the AKR labelled by Rhodamine B were distributed solely at the oil/water interfaces, with only a fluorescent circle being observed around droplets (Figure 1E and Figure S4). NADP$^+$ on its own is not fluorescent. However, its reductive state (NADPH) is fluorescent and was accordingly used for fluorescent observation. Strong fluorescent signals were observed throughout the droplets (Figure 1F and Figure S4), indicating that NADPH molecules are homogeneously distributed within the droplets. Since NADP$^+$ bears one more charge than NADPH, NADP$^+$ is thereby believed to be more water-soluble. As such, it is safe to infer that NADP$^+$ molecules are also distributed within the interior of water droplets. To further check the compartmentalization ability of droplets towards the enzymes and cofactors, the Pickering emulsion droplets-based fixed reactor was treated with flowing *n*-heptane (5 mL h^{-1}). After 48 h of continuous flow, it was found that 93.0% of the initial AKR and 97.5% of the initial NADP$^+$ were retained within the fixed-bed reactors (Figure S5). This provides preliminary confirmation of the good compartmentalization ability of the droplets towards the enzymes and cofactors. Moreover, our co-compartmentalization method for the co-immobilization of enzymes and cofactors is straightforward nonetheless efficient, because the enzymes and cofactors added are nearly completely transferred to the fixed-bed reactor through a one-step emulsion. This was done without need for any covalent linkages or ionic pair interactions, as currently required by other existing methods.[4] Moreover, the loadings of enzymes and cofactors can be facilely tuned by changing their amounts added.

To benchmark the proposed continuous flow system, we first examined a conventional biphasic system and Pickering emulsion system in batch, using 2-chloro-3',4'-difluoroacetophenone (0.1 M) as substrate and 2-octanol as co-substrate (Figure 2A). It was found that 2-octanol was a good co-substrate (hydrogen-donor) for our system (Figure S6) and that 0.24 M 2-octanol was sufficient to regenerate NADP$^+$ (Figure S7). In the conventional biphasic system, a 91% conversion and the product (S)-2-chloro-1-(3,4-difluorophenyl) ethanol in >99 ee% were obtained after 7 h of reaction (Figure 2B). According to the conversion, the catalytic efficiency of AKR (CE_e) in this system was calculated to be 0.10 U mg^{-1}. For the Pickering emulsion system in batch, the conversion of 2-chloro-3',4'-difluoroacetophenone was 93% after the same period (Figure 2C), slightly higher than the biphasic batch system although the ee values obtained in these two cases are at the same level. In this case, the CE_e was estimated to be 0.11 U mg^{-1}, which is only slightly higher than the one obtained in the conventional biphasic system. Interestingly, in our continuous flow system, the conversion of 2-chloro-3',4'-difluoroacetophenone at steady-state was more than 98% and ee% of (S)-2-chloro-1-(3,4-difluorophenyl)ethanol was maintained at 99% (Figure 2D). The CE_e reached a value as high as 0.269 U mg^{-1}, which is 2.7-fold or 2.6-fold higher than those obtained in the typical biphasic system and the Pickering emulsion system in batch, respectively (Figure 2E). The same trend was seen in the case of another substrate, ethyl 4-

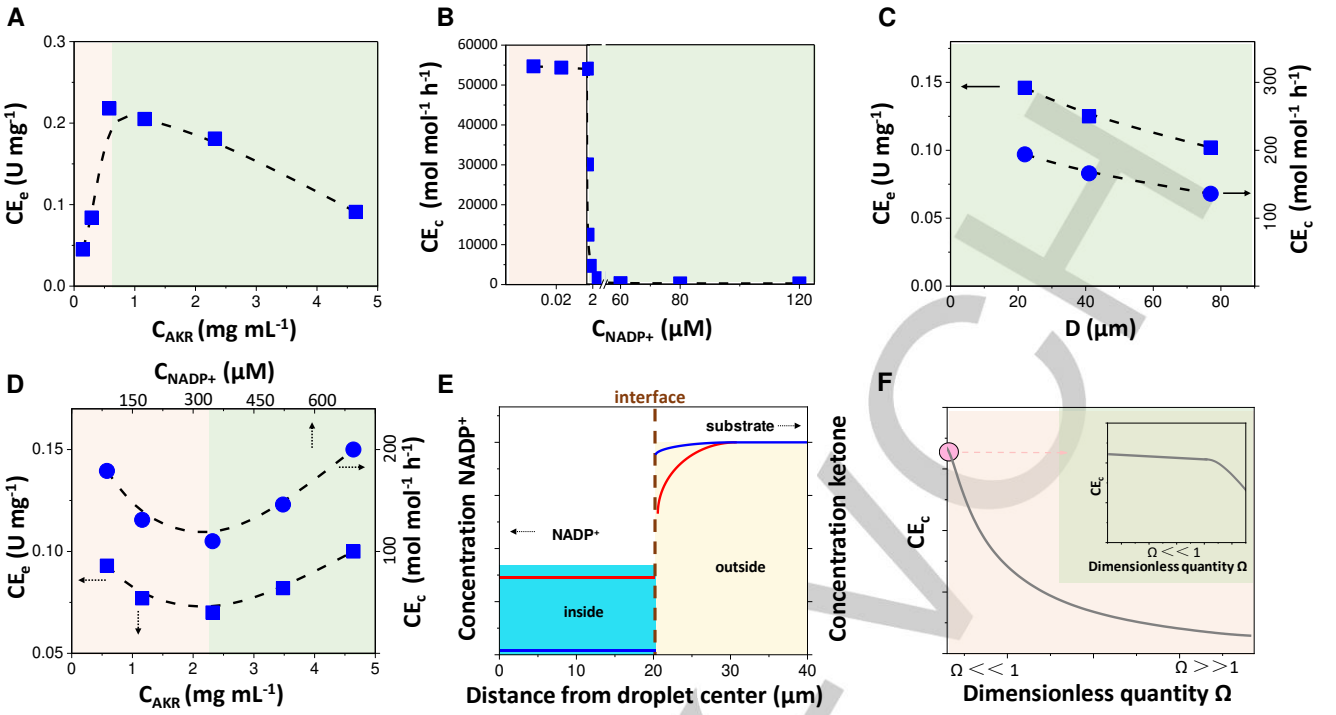

Figure 3. Impacts of key reaction conditions on the reaction efficiency of Pickering emulsion-based continuous flow system. A) Catalytic efficiency of AKR (CE_e) as a function of its concentration (the amount of AKR is changed). B) Catalytic efficiency of NADP$^+$ (CE_c, mol of product produced per mol of cofactor per h) as a function of its concentration. C) Catalytic efficiency of AKR and catalytic efficiency of NADP$^+$ as a function of the droplet size. D) Catalytic efficiency of AKR and catalytic efficiency of NADP$^+$ as a function of their respective concentrations (the amounts of AKR and NADP$^+$ are fixed). E) Predicted concentration distributions of NADP$^+$ and the substrate within the Pickering emulsion system. F) The calculated relationship between the dimensionless quantity Ω and catalytic efficiency of NADP$^+$. The inset shows the trends of CE_c when $\Omega \ll 1$. Reaction conditions are provided in Supporting Information.

chloroacetoacetate (Figure 2F and Figure S8). The CE_e in the flow system is 2.9-fold or 2.6-fold higher than those obtained in the conventional biphasic system and the Pickering emulsion system in batch, respectively. These results underline an enhancement in catalytic efficiency obtained in our continuous flow system. This enhancement is probably attributed to the continuous flow effect that can result in timely removal of the product from the reaction system and thereby pushes the reaction in the forward direction. This inference is supported by the experiments at different flow rates (Figure 2G and Figure S9). When the flow rate was increased from 0.5 to 1.0 and further to 2.0 mL h^{-1}, the CE_e increased from 0.20 (93%) to 0.34 (80%) and then 0.40 (68%) U mg^{-1}. Moreover, it was found that the specific activity of AKR (the specific activity is determined in a kinetic region of the conversion linearly increasing with time) was 22.4-fold or 5.1-fold higher than those obtained in the typical biphasic system and the Pickering emulsion batch system (Figure S10). The specific activity determined at different flow rates also supports that the continuous flow can result in timely removal of the product from the reaction system, leading to a high efficiency (Figure S11). These results highlight the benefits of our Pickering emulsion droplet-based continuous flow system.

To get insights into the enzymatic reactions occurring within the compartmentalized systems, we tested a series of reactions under different reaction conditions. Firstly, we changed the concentration of AKR over a very wide range (0.145 to 4.64 mg mL^{-1}, Figure S12) while fixing the NADP$^+$ concentration at 80 μM (When the concentration of NADP$^+$ is more than 80 □M, the experimental results show that the amount of NADP$^+$ no longer affect the CE_e because the cofactor is excessive). As shown in Figure 3A, the CE_e rapidly increased at first, reached a maximum (0.22 U mg^{-1}) at 0.58 mg mL^{-1}, and then began to decrease. This pronounced concentration-dependent effect is explained in terms of the changes in the location of AKR in the Pickering emulsion system. It was found that a small amount of AKR were adsorbed at the silica emulsifier surface through chemical interactions with Si-OH on the silica surface (Figure S13). At very low enzyme concentrations, the chemically adsorbed AKR accounts for a relatively large fraction because the total amount was very small. This scenario led to a relatively low accessibility of AKR towards cofactors. As the AKR concentration increases, most of AKR molecules are gradually adsorbed at the oil/water interfaces, representing a dominant distribution. In this case, most of enzymes are adsorbed at the interphase intercalating the solid particles (Figures S14 and S15; Nevertheless, even in the presence of concentrated enzymes as high as 4.64 mg mL^{-1}, our Pickering emulsion droplets-based continuous flow system still has a good operational stability, as shown in Figure S16).[10] This case results in high enzyme accessibility for cofactors and substrates, giving rise to a high catalytic efficiency. However, once the AKR concentration is beyond the threshold value (0.58 mg mL^{-1}) corresponding to the saturated monolayer adsorption, multilayer adsorption occurs. This threshold value is close to the value estimated from the interfacial tension measurement results. These findings mirror one characteristic of our system, the strong dependence on the enzyme interfacial adsorption arising from the Pickering emulsion droplet compartmentalization.

In order to get further insights into the co-compartmentalization effects, it is also rewarding to consider the impact of the NADP$^+$ concentration and the droplet size on the reaction efficiency, i.e. the catalytic efficiency of enzyme (CE_e) or the catalytic efficiency of NADP$^+$ (CE_c). This was investigated by varying the

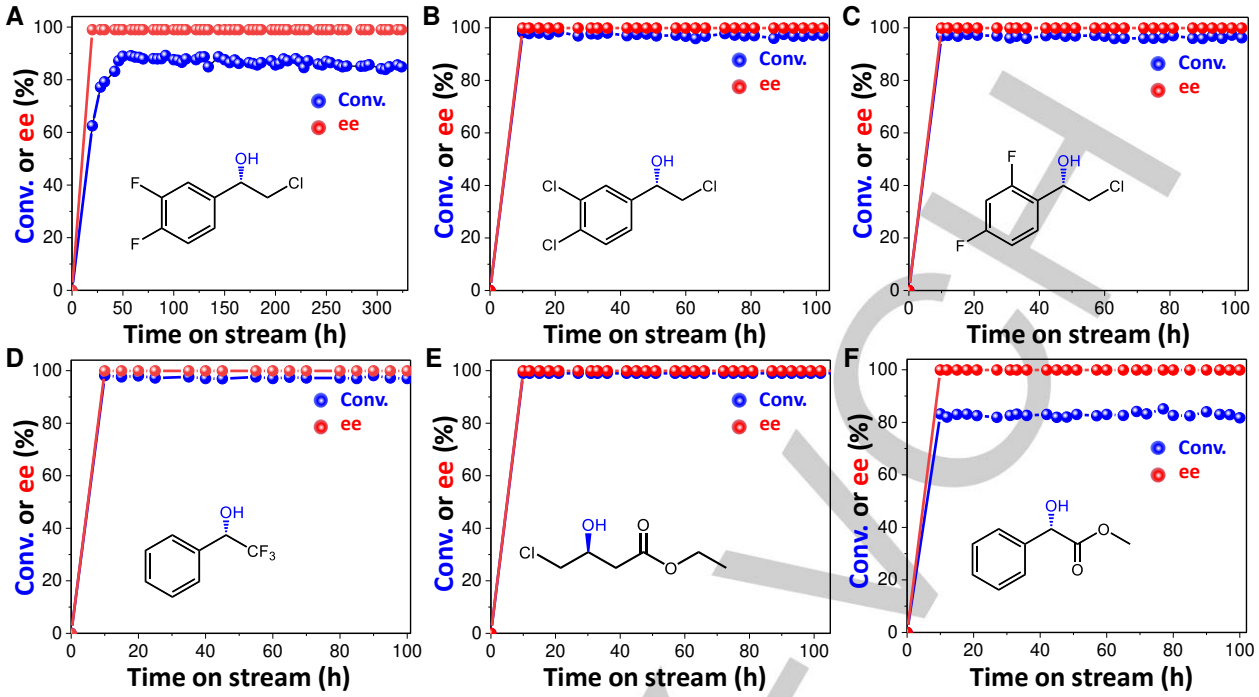

Figure 4. Enzymatic reduction of various ketones in the Pickering emulsion-based continuous flow systems. A) 2-Chloro-3',4'-difluoroacetophenone. B) 2,3',4'-Trichloroacetophenone. C) 2-Chloro-2',4'-difluoroacetophenone. D) 2,2,2-Trifluoroacetophenone. E) Ethyl 4-chloroacetoacetate. F) Methyl benzoylformate. Reaction conditions: Pickering emulsions consist of 1.8 mL of *n*-heptane, 3.6 mL of aqueous AKR (0.58 mg mL^{-1}) and $NADP^+$ (80 μM) and 0.15 g of emulsifier, 0.10 M ketone, 0.24 M 2-octanol, *n*-heptane as mobile phase, 30 °C, flow rate (1.0 mL h^{-1}). For the case of 2,2,2-trifluoroacetophenone, the concentrations of AKR and $NADP^+$ are 2.32 mg mL^{-1} and 320 μM, respectively. For 2-chloro-3',4'-difluoroacetophenone, the flow rate is 1.0 mL h^{-1} at the beginning of reaction, 0.5 mL h^{-1} after 200 h. For ethyl 4-chloroacetoacetate, the flow rate is 1.5 mL h^{-1}.

concentration of $NADP^+$ from 0.011 to 120 μM while keeping the concentration of AKR and the total volume of Pickering emulsion fixed (Figure S17). The CE_c was observed to be almost constant when the concentration of $NADP^+$ was less than 0.033 μM. However, as the $NADP^+$ concentration increased from 0.033 to 80 μM, the CE_c rapidly decreased (Figure 3B); when $NADP^+$ concentration is beyond 80 μM, the CE_c gradually leveled off. The reason for such a concentration-dependent effect is explained in the coming theoretical analysis. Moreover, since the enzymatic reactions take place at the surfaces of droplets, we carefully adjusted the droplet size to observe the changes in the CE_e and CE_c (their concentrations were fixed). The droplet size was tuned by changing emulsification conditions (See Experimental Section in the Supporting Information). As Figure 3C displays, when the droplet size was decreased from 77 to 23 μm (Figure S18), the CE_e increased from 0.10 to 0.146 U mg^{-1} and the CE_c also increased from 141 to 201 mol mol^{-1} h^{-1}. Such changes are understandable because the smaller droplet size means a higher interfacial area available for reactions. Inspired by these concentration effects, we were interested in investigating the impact of the AKR and $NADP^+$ local concentrations on the reaction efficiency while maintaining their respective total amounts constant (Figure S19, their molar ratio is fixed at about 1:4). With the increase in the local concentration of AKR, the CE_e first decreased, reduced to a lowest point, and then began to rebound (Figure 3D). Similarly, the CE_c first decreased to a lowest value and then increased as its location concentration increased. There are two factors governing these observed changes. Since the amounts of AKR and $NADP^+$ were not changed, increasing the local concentrations means decreasing the number of droplets, further leading to a reduction in interfacial areas available for reactions. This is unfavorable for the enzymatic reactions. At the same time, increasing the local concentration results in shortening the average distances between the enzymes and cofactors, thereby favoring their coming into contact with each other. Such a trade-off between the interfacial area effects and the average distance effects may give rise to the presence of a lowest efficiency.

In order to rationalize some of the unique effects seen above, we established a generalized theoretical model to mathematically analyze the reactions occurring in such a system. The model is depicted in the Supporting Information. According to the enzymatic reactions investigated here, we consider two reactions in series involving: A + B ↔ C + D for the product generation and E + D ↔ F + B for the cofactor regeneration. Here, A represents the substrate, B the cofactor at reductive state, C the product, D the cofactor at oxidative state, E the co-substrate and F the co-product. A, C, E and F are all oil-soluble but highly insoluble in water, whereas B and D are highly water-soluble, thereby only being confined within the water droplets. These two reactions both occur at the interface of droplets, as the enzymes are located at these positions. The reaction constants for the forward reactions, per unit surface area, are denoted by k_1 and k_3 for the two reactions, respectively. The backward reactions can safely be ignored as there are no catalytic reactions taking place in bulk water or oil. The rate of conversions of B to D or vice versa, as occurring on the surface of droplets, is dominated by the forward reactions rather than the backward ones. The concentration profiles within both oil and water phases are governed by the diffusion equation:

$$\frac{\partial X}{\partial t} = d_f^i \nabla^2 X \qquad (1)$$

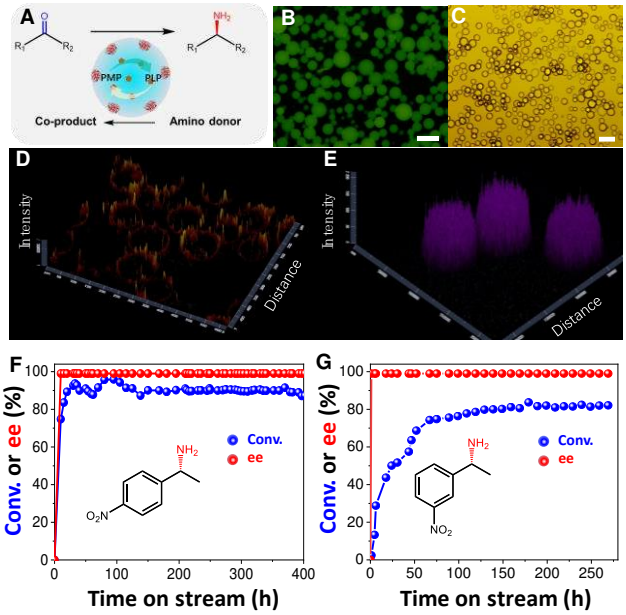

Figure 5. Co-compartmentalization of transaminase and PLP within Pickering emulsion droplets for continuous flow reactions. A) Scheme showing the enantioselective transamination of ketones. B) Optical microscopy image of the prepared Pickering emulsion droplets. C) Fluorescence confocal microscopy image of the droplets dyed by water-soluble FITC-dextran. D, E) 2.5D confocal fluorescence microscopy for the distribution of Rhodamine B-labelled enzyme or PLP cofactor within the droplets. Scale bar = 100 μm. F, G) Continuous flow transamination of 4'-nitroacetophenone and 3'-nitroacetophenone. Reaction conditions: Pickering emulsions consist of 3 mL of toluene, 6 mL of 0.36 (F) or 1.44 mg mL^{-1} TA (G), 0.75 (F) or 3.0 mM PLP (G) and 0.18 g of emulsifier, 0.05 M ketone and 0.2 M phenylethylamine in toluene as mobile phase, 45 °C, flow rate (0.5 mL h^{-1} at the beginning of reaction, 0.3 mL h^{-1} after 200 h).

where X = A, B, C, D, E, or F represents the concentration of each component, and d_f^i is the diffusion coefficient with i = o or w, depending on whether the component resides in water (B and D) or in the oil phase (A, C, E, and F). Under steady-state conditions, all time-dependent variations of the concentration profiles vanish. Under such circumstances equation (1) reduces to $\nabla^2 X = 0$, which has the well-known radial solution of the form:

$$X(r) = b_1^x + \frac{b_2^x}{r} \qquad (2)$$

for the profile around a droplet, with r representing the distance measured from the centre of the droplet. For given bulk concentrations of reactants A and E in the oil phase, denoted here as A_∞ and E_∞ from now on, we have constants $b_1^a = A_\infty$ and $b_1^e = E_\infty$, for components A and E respectively. The constant b_2 in each case is obtained by considering the consumption rates of A and E at the interfaces and equating these to the diffusion rates of each molecule moving from the bulk oil phase to the surface of the droplets. These rates will depend on the concentrations of A and E on the surface of droplets, A_R and E_R. However, when r is equal to R, then equation (2) should also evaluate to A_R or E_R, depending on which component is being considered. These relations can be used (see Supporting Information) to derive the following expressions, relating concentrations of A or E on the surface of droplets to their respective bulk concentrations, under steady-state conditions:

$$A_R = \left(1 + \frac{k_1 BR}{d_f^0}\right)^{-1} A_\infty \qquad (3)$$

$$E_R = \left(1 + \frac{k_3 DR}{d_f^0}\right)^{-1} E_\infty \qquad (4)$$

The rate of conversion per initial mole of B, represented here by δ, under the same steady-state conditions, can now also be calculated and is given by (for detailed derivation in the Supporting Information):

$$\delta = \left(\frac{\theta}{1+\Omega\theta}\right)\frac{\left(4\pi R^2 k_1 A_\infty B^{in}\right)}{\frac{4}{3}\pi R^3 B^{in}} = \left(\frac{\theta}{1+\Omega\theta}\right)\frac{3k_1 A_\infty}{R} \qquad (5)$$

where we have defined two important parameters $\Omega = \frac{k_1 R B^{in}}{d_f^o}$ and $\theta = \frac{k_3 E_\infty}{(k_3 E_\infty + k_1 A_\infty)}$ characterizing the system.

Equation (5) demonstrates that at low initial concentrations of B, i.e. small values of B^{in}, the conversion of A to C on the droplet surface is very slow and the reactions on the interface are the main rate-limiting steps. Consequently, as equation (3) indicates, the concentration of A at the interface is also only slightly lower than that in the bulk oil phase. However, at higher concentrations B^{in}, the conversion of A to C on the surface of droplets is very fast. The diffusion of A and E from the bulk oil phase to the interface of droplets now becomes the main rate-limiting step. As a result, the concentration of A at the interface is significantly lower in comparison to the bulk concentration in the oil phase. Our theoretic analysis is graphically illustrated in Figure 3E, where the concentration of B on one side of the interface (water side) and that of A on the other side (oil phase) have been schematically depicted. The figure shows how the latter alters as B^{in} is changed from a low (blue line) to a high value (red line).

As equation (5) shows, the catalytic efficiency of cofactor, δ, is affected by the dimensionless quantity Ω. Roughly speaking, this parameter represents the ratio of the rate of consumption of A on the surface of droplets to the rate of arrival (driven by diffusion) of A from the bulk oil phase to the droplet interfaces. The parameter θ, on the other hand, indicates the proportion of B (out of an initial concentration of B^{in}) inside the droplets at steady-state. The remainder of initial B is present as converted to D under the same conditions. Most importantly, at low initial concentrations (small B^{in}), where $\Omega \ll 1$, we have $\delta \to (3\theta k_1 A_\infty) / R$ which as can be noted is completely independent of B^{in}. As such, δ is accordingly almost constant, as shown in Figure 3F. This is almost consistent with our experimental observations (Figure 3B). At larger concentrations B^{in}, where now $\Omega \gg 1$, $\delta \approx 3\, d_f^0 A_\infty / R^2 B^{in}$. This means δ decreases as $1/B^{in}$. In this same regime, the improvement in the specificity with the smaller size of droplets is found, varying as $1 / R^2$. Some experimental supports for these predicted trends can be seen in Figures 3B and 3C. These established equations with key theoretical parameters can help us to rationally understand the changes of reaction results in the relatively complex network, and further serve to guide optimization of reaction conditions such as substrate concentration, cofactor concentration and droplet size.

Quite impressively, the co-compartmentalized system worked well in a fixed-bed fashion. For the reduction of 2-chloro-3',4'-difluoroacetophenone to high-value (S)-2-chloro-1-(3,4-difluorophenyl)ethanol, the conversion was always maintained at 90% during a period of 300 h (Figure 4A), albeit at the expense of the flow rate. More than 99% ee chiral alcohol was afforded during this long period. The space-time yield was estimated to be 133 mg mL^{-1} day^{-1} (for 100 mM substrate). Such a value is at a moderate level in comparison to the reported values.[3,4] This is because our Pickering emulsion-based continuous flow system includes a given volume of buffer solution serving as a physiological microenvironment for enzymes, which accounts for

a large portion of the total volume of the fixed-bed reactor. Notably, the total turnover number (TTN, mol mol^{-1}) of NADPH reached 59204 mol mol^{-1}, which is much higher than most of ever reported results (Table S1). The productivity of the AKR (grams of product obtained per gram of enzyme) is as high as 2.73 g mg^{-1} for 300 h of continuous reaction. Over the period of time studied, no further $NADP^+$ was needed to be added into the system after starting the reaction. That is to say, our reaction system is a cofactor self-sufficient system in that the formed $NADP^+$ is converted back to NADPH within the water droplets by AKR-catalyzed oxidation of 2-octanol to 2-octanone (Figure S20). After the long period of operation, the droplets are virtually unchanged in respect to the morphology and sizes, when compared with the droplets before the start of the reactions (Figure S21). After such a long time, no significant loss of the cofactor was detected, as confirmed by UV-Vis measurements (Figure S22a). Similarly, 89% of the initial AKR was still retained inside the fixed-bed reactor according to the results obtained from Bradford method (Figure S22b; the portion of the enzymes that adsorbed on the emulsifiers was eliminated as indicated in Figure S13). These results exclude the possibility of the decrease in catalytic efficiency being caused by the leaching of the enzyme and cofactors. To gain more information about the decrease in catalytic efficiency, we conducted two sets of control experiments. Firstly, after an aqueous solution of AKR was left standing for 300 h, cofactors, substrate and co-substrate were added to the system, but almost no substrate was converted. However, after the $NADP^+$ solution was left standing for 300 h, a 92% conversion was obtained (Figure S23). These results point to the fact that the decrease in catalytic efficiency is caused by the deactivation of AKR instead of $NADP^+$. Secondly, after an aqueous solution containing AKR, $NADP^+$ and emulsifier was left standing at 30 °C for 75 h, the substrate and co-substrate were then added. Again, no product was detected (Figure S24). When a *n*-heptane/water biphasic system containing AKR and $NADP^+$ was left standing at 30 °C for 75 h, only a conversion of 1% was achieved within 6 h. In contrast, when a Pickering emulsion system containing AKR and $NADP^+$ was left standing under the same conditions, the conversion was 12%, much higher than those obtained in the former two systems. These comparative outcomes indicate that the presence of Pickering emulsion interfaces is favorable for maintaining the enzyme activity. A possible explanation for this is that the strong adsorption of enzymes at the Pickering emulsion interfaces reduces the risk of enzyme aggregation which often occurs in the bulk water phase.[11] This view is indeed supported by our experimental observations. This interesting finding would be very important in practical applications. Our flow system works well for synthesis of a series of high-value chiral alcohols. For 2,3',4'-trichloroacetophenone (Figure 4B), 2-chloro-2',4'-difluoroacetophenone (Figure 4C), 2,2,2-trifluroacetophenone (Figure 4D) and ethyl 4-chloroacetoacetate (Figure 4E), the conversions were maintained above 95% and the ee values for all the generated alcohols were also above 99%, following 100 h of continuous operation. Even for the less reactive substrates such as methyl benzoylformate, 80% conversion and >99 ee% were achieved during the 100 h of continuous flow (Figure 4F).

To examine the generality of our co-compartmentalized system for the continuous utilization of enzymes and cofactors, we conducted transamination reactions for synthesis of chiral amines, which is among the most industrially important chiral reactions (Figure 5A).[12] This reaction involves transaminase (Figure S25) and PLP (cofactor). Similar to the enzymatic ketone reduction, transaminases were dominantly adsorbed at the oil/water interface, whereas the cofactor PLP is distributed in the interior of the water droplets, as affirmed by fluorescent observations (Figures 5B-E and Figure S26). In the continuous flow system, the conversion of 4'-nitroacetophenone was kept at above 88%, with the ee values for (R)-1-(4-nitrophenyl)ethanamine always being >99% during 400 h of continuous flow operation (Figure 5F). The CE_e in the flow system is *ca.* 2-fold higher than those obtained in the conventional biphasic system and the Pickering emulsion system in batch (Figure S27). For another substrate, 3'-nitroacetophenone, the conversion and ee values were always maintained above 80% and 99% during 280 h of continuous reaction (Figure 5G). These demonstrations further confirmed that our co-compartmentalized system is versatile and efficient for continuous flow reactions involving both enzymes and cofactors.

Conclusion

In conclusion, we have successfully developed a novel continuous flow biocatalysis system based on the co-compartmentalization of enzymes and cofactors within Pickering emulsion droplets. The key to such a success is the judicious use of the droplets which can confine the water-soluble cofactors in their interior while having the enzymes strongly adsorbed at their surface, thereby realizing the co-compartmentalization of enzymes and cofactors within micro-scaled spaces. This unique system allows the cofactors to freely access the enzymes and be fully regenerated within the droplets, hence representing a new model for the co-immobilization of enzymes and cofactors. As demonstrated by NADPH-dependent ketone reductions and PLP-dependent transamination reactions, in comparison to the conventional biphasic reaction, the Pickering emulsion-based continuous flow system works more efficiently, with serval-fold enhancement in catalytic efficiency. Impressively, the system exhibits excellent stability (even after 300~400 h of continuous operation) and an outstanding TTN (59204 mol mol^{-1} for enzymatic ketone reduction), which are much better than the reported results. Moreover, our established theoretic model further reveals the features of this system and provides a deeper understanding of the compartmentalization effects. Being operationally straightforward and cofactor self-sufficient, our method along with the insights into co-compartmentalization of enzymes and cofactors, provides a great opportunity for a step change advancement towards the use of continuous flow biocatalysis in more practically orientated applications.

Acknowledgements

This work was supported by the Natural Science Foundation of China (21925203 and 21733009), Program for Youth Sanjin Scholar, 100 Talent Project of Shanxi Province, and the Fund for Shanxi “1331 Project”.

Conflict of interest

The authors declare no conflict of interest.

Keywords: Pickering emulsions • Continuous flow catalysis • Interfacial reactions • Biphasic reactions

[1] a) B. Gutmann, D. Cantillo, C. O. Kappe, *Angew. Chem. Int. Ed.* **2015**, *54*, 6688–6728; b) B. Pieber, M. Shalom, M. Antonietti, P. H. Seeberger, K. Gilmore, *Angew. Chem. Int. Ed.* **2018**, *57*, 9976–9979; c) R. Greifenstein, T. Ballweg, T. Hashem, E. Gottwald, D. Achauer, F. Kirschhöfer, M. Nusser, G. Brenner-Weiss, E. Sedghamiz, W. Wenzel, E. Mittmann, K. S. Rabe, C. M. Niemeyer, M. Franzreb, C. Wöll, *Angew. Chem. Int. Ed.* **2022**, *61,* e20211714; d) J. Britton, R. P. Dyer, S. Majumdar, C. L. Raston, G. A. Weiss, *Angew. Chem. Int. Ed.* **2017**, *56*, 2296–2301; e) J. Britton, S. Majumdar, G. A. Weiss, *Chem. Soc. Rev.* **2018**, *47*, 5891–5918; f) M. Romero-Fernández, F. Paradisi, *Curr. Opin. Chem. Biol.* **2020**, *55*, 1–8; g) L. Tamborini, P. Fernandes, F. Paradisi, F. Molinari, *Trends Biotechnol.* **2018**, *36*, 73–88; h) S. Kundu, A. S. Bhangale, W. E. Wallace, K. M. Flynn, C. M. Guttman, R. A. Gross, K. L. Beers, *J. Am. Chem. Soc.* **2011**, *133*, 6006–6011; i) A. Adamo, R. L. Beingessner, M. Behnam, J. Chen, T. F. Jamison, K. F. Jensen, J. M. Monbaliu, A. S. Myerson, E. M. Revalor, D. R. Snead, T. Stelzer, N. Weeranoppanant, S. Y. Wong, P. Zhang, *Science* **2016**, *352*, 61–67.

[2] a) S. Wu, R. Snajdrova, J. C. Moore, K. Baldenius, U. T. Bornscheuer, *Angew. Chem. Int. Ed.* **2021**, *60*, 88–119; b) R. A. Sheldon, S. Van Pelt, *Chem. Soc. Rev.* **2013**, *42*, 6223–6235; c) P. Jonkheijm, D. Weinrich, H. Schrder, C. M. Niemeyer, H. Waldmann, *Angew. Chem. Int. Ed.* **2008**, *47*, 9618–9647; d) U. Hanefeld, F. Hollmann, C. E. Paul, *Chem. Soc. Rev.* **2022**, *51*, 594–627; e) C. Hu, Z. Huang, M. Jiang, Y. Tao, Z. Li, X. Wu, D. Cheng, F. Chen, *ACS Sustainable Chem. Eng.* **2021**, *9*, 8990−9000.

[3] a) J. Liang, S. Gao, J. Liu, M. Y. B. Zulkifli, J. Xu, J. Scott, V. C. Chen, J. Shi, A. Rawal, K. Liang, *Angew. Chem. Int. Ed.* **2021**, *60*, 5421–5428; b) Y. Q. Zhang, T. T. Feng, Y. F. Cao, X. Y. Zhang, T. Wang, M. R. H. Nina, L. C. Wang, H. L. Yu, J. H. Xu, J. Ge, Y. P. Bai, *ACS Catal.* **2021**, *11*, 10487−10493; c) T. Peschke, M. Skoupi, T. Burgahn, S. Gallus, I. Ahmed, K. S. Rabe, C. M. Niemeyer, *ACS Catal.* **2017**, *7*, 7866−7872; d) T. Peschke, P. Bitterwolf, S. Gallus, Y. Hu, C. Oelschlaeger, N. Willenbacher, K. S. Rabe, C. M. Niemeyer, *Angew. Chem. Int. Ed.* **2018**, *57*, 17028–17032.

[4] a) S. Velasco-Lozano, A. I. Benítez-Mateos, F. López-Gallego, *Angew. Chem. Int. Ed.* **2017**, *56*, 771–775; b) C. J. Hartley, C. C. Williams, J. A. Scoble, Q. I. Churches, A. North, N. G. French, T. Nebl, G. Coia, A. C. Warden, G. Simpson, A. R. Frazer, C. N. Jensen, N. J. Turner, C. Scott, *Nat. Catal.* **2019**, *2*, 1006–1015; c) A. I. Benítez-Mateos, M. L. Contente, S. Velasco-Lozano, F. Paradisi, F. López-Gallego, *ACS Sustainable Chem. Eng.* **2018**, *6*, 13151−13159; d) H. Zhao, W. A. Van Der Donk, *Curr. Opin. Biotechnol.* **2003**, *14*, 583–589; e) L. Nagy-Győr, E. Abaházi, V. Bódai, P. Sátorhelyi, B. Erdélyi, D. Balogh-Weiser, C. Paizs, G. Hornyánszky, L. Poppe, *ChemBioChem* **2018**, *19*, 1845–1848; f) W. Liu, P. Wang, *Biotechnol. Adv.* **2007**, *25*, 369–384; g) B. Baumer, T. Classen, M. Pohl, J. Pietruszka, *Adv. Synth. Catal.* **2020**, *362*, 2894–2901; h) A. P. Mattey, G. J. Ford, J. Citoler, C. Baldwin, J. R. Marshall, R. B. Palmer, M. Thompson, N. J. Turner, S. C. Cosgrove, S. L. Flitsch, *Angew. Chem. Int. Ed.* **2021** ,*60*, 18660–18665; i) M. Zoumpanioti, H. Stamatis, A. Xenakis, *Biotechnol. Adv.* **2010**, *28*, 395–406; j) C. Wu, S. Bai, M. B. Ansorge-Schumacher, D. Wang, *Adv. Mater.* **2011**, *23*, 5694–5699.

[5] a) M. Pera-Titus, L. Leclercq, J. M. Clacens, F. De Campo, V. Nardello-Rataj, *Angew. Chem. Int. Ed.* **2015**, *54*, 2006–2021; b) Z. Sun, U. Glebe, H. Charan, A. Bçker, C. Wu, *Angew. Chem. Int. Ed.* **2018**, *57*, 13810–13814; c) J. Potier, S. Menuel, M. H. Chambrier, L. Burylo, J. F. Blach, P. Woisel, E. Monflier, F. Hapiot, *ACS Catal.* **2013**, *3*, 1618–1621; d) M. Kim, S. J. Yeo, C. B. Highley, J. A. Burdick, P. J. Yoo, J. Doh, D. Lee, *ACS Nano* **2015**, *9*, 8269–8278; e) H. Jiang, Y. Li, L. Hong, T. Ngai, *Chem. Asian J.* **2018**, *13*, 3533–3539; f) Q. Wei, C. Yu, X. Song, Y. Zhong, L. Ni, Y. Ren, W. Guo, J. Yu, J. Qiu, *J. Am. Chem. Soc.* **2021**, *143*, 6071−6078; g) H. Wu, X. Du, X. Meng, D. Qiu, Y. Qiao, *Nat. Commun.* **2021**, *12*, 6113; h) Z. Wang, M. C. M. Van Oers, F. P. J. T. Rutjes, J. C. M. Van Hest, *Angew. Chem. Int. Ed.* **2012**, *51*, 10746–10750; i) P. A. Zapata, J. Faria, M. P. Ruiz, R. E. Jentoft, D. E. Resasco, *J. Am. Chem. Soc.* **2012**, *134*, 8570–8578.

[6] a) M. Zhang, L. Wei, H. Chen, Z. Du, B. P. Binks, H. Yang, *J. Am. Chem. Soc.* **2016**, *138,* 10173−10183; b) M. Zhang, R. Ettelaie, T. Yan, S. Zhang, F. Cheng, B. P. Binks, H. Yang, *J. Am. Chem. Soc.* **2017**, *139*, 17387−17396.

[7] a) Z. Li, H. Yang, J. Liu, Z. Huang, F. Chen, *Chem. Rec.* **2021**, *21*, 1611–1630; b) M. L. Contente, F. Paradisi, *Nat. Catal.* **2018**, *1*, 452–459; c) M. Heidlindemann, G. Rulli, A. Berkessel, W. Hummel, H. Gröger, *ACS Catal.* **2014**, *4*, 1099−1103; d) J. Cao, T. K. Hyster, *ACS Catal.* **2020**, *10*, 6171−6175; e) F. Hollmann, I. W. C. E. Arendsa, D. Holtmannb, *Green Chem.* **2011**, *13*, 2285–2313; f) X. Chen, L. Xu, A. Wang, H. Li, C. Wang, X. Pei, P. Zhang, S. G. Wu, *J Chem Technol Biotechnol* **2019**, *94*, 236–243.

[8] a) C. J. Beverung, C. J. Radke, H. W. Blanch, *Biophysical Chemistry* **1999**, *81*, 59–80; b) S. Rusli, J. Grabowski, A. Drews, M. Kraume, *Processes* **2020**, *8*, 1082; c) J. Maldonado-Valderrama, V. B. Fainerman, E. Aksenenko, M. J. Galvez-Ruiz, M. A. Cabrerizo-Vílchez, R. Miller, *Colloids Surf. A* **2005**, *261*, 85–92.

[9] E. Diamanti, J. Santiago-Arcos, D. Grajales-Hernández, N. Czarnievicz, N. Comino, I. Llarena, D. D. Silvio, A. L. Cortajarena, F. López-Gallego, *ACS Catal.* **2021,** *11,* 15051-15067.

[10] a) A. Heysea, C. Plikatb, M. Grüna, S. Delavala, M. Ansorge-Schumacherb, A. Drews, *Process Biochem.* **2018**, *72*, 86-95; b) C. Plikat, A. Drews, M. B. Ansorge-Schumacher, *ChemCatChem* **2022**, e202200444. c) S. Tcholakova, N. D. Denkov, A. Lips, *Phys. Chem. Chem. Phys.* **2008**, *10*, 1608–1627; d) A. Sarkar, B. Murray, M. Holmes, R. Ettelaie, A. Abdalla, X. Yang, *Soft Matter* **2016**, *12,* 3558-3569.

[11] a) L. Day, J. Zhai, M. Xu, N. C. Jones, S. V. Hoffmann, T. J. Wooster, *Food Hydrocoll.* **2014**, *34*, 78–87; b) E. Dickinson, *Colloid Surf. B-Biointerfaces* **2010**, *81*, 130–140; c) S. Das, S. Behera, S. Balasubramanian, *J. Phys. Chem. Lett.* **2020**, *11*, 2977−2982.

[12] a) R. C. Simon, N. Richter, E. Busto, W. Kroutil, *ACS Catal.* **2014**, *4*, 129−143; b) S. A. Kelly, S. Pohle, S. Wharry, S. Mix, C. C. R. Allen, T. S. Moody, B. F. Gilmore, *Chem. Rev.* **2018**, *118*, 349−367; c) F. G. Mutti, T. Knaus, N. S. Scrutton, M. Breuer, N. J. Turner, *Science* **2015**, *349*, 1525–1529; d) I. V. Pavlidis, M. S. Weiss, M. Genz, P. Spurr, S. P. Hanlon, B. Wirz, H. Iding, U. T. Bornscheuer, *Nat. Chem.* **2016**, *8*, 1076–1082; e) L. Marx, N. Ríos-Lombardía, J. F. Farnberger, W. Kroutil, A. I. Benítez-Mateos, F. López-Gallego, F. Morís, J. González-Sabín, P. Berglund, *Adv. Synth. Catal.* **2018**, *360*, 2157–2165.

Entry for the Table of Contents

A novel continuous flow biocatalysis based on the co-compartmentalization of enzymes and cofactors within Pickering emulsion droplets comes out. As exemplified by enzyme-catalyzed ketone enantioselective reduction and enantioselective transamination, this system features long-term operational stability, excellent catalytic efficiency and no need for exogenous cofactors.